TISSUE ENGINEERING: Part A
Volume 18, Numbers 23 and 24, 2012

DOI: 10.1089/ten.tea.2011.0594

A Nonhuman Primate Model of Lung Regeneration: Detergent-Mediated Decellularization and Initial *In Vitro* Recellularization with Mesenchymal Stem Cells

Ryan W. Bonvillain, Ph.D.,[1] Svitlana Danchuk, M.S.,[1] Deborah E. Sullivan, Ph.D.,[1,2] Aline M. Betancourt, Ph.D.,[1,2] Julie A. Semon, Ph.D.,[1] Michelle E. Eagle, B.S.,[1] Jacques P. Mayeux, B.S.,[1] Ashley N. Gregory,[1] Guangdi Wang, Ph.D.,[3] Ian K. Townley, Ph.D.,[3] Zachary D. Borg, B.S.,[4] Daniel J. Weiss, M.D., Ph.D.,[4] and Bruce A. Bunnell, Ph.D.[1,5]

Currently, patients with end-stage lung disease are limited to lung transplantation as their only treatment option. Unfortunately, the lungs available for transplantation are few. Moreover, transplant recipients require life-long immune suppression to tolerate the transplanted lung. A promising alternative therapeutic strategy is decellularization of whole lungs, which permits the isolation of an intact scaffold comprised of innate extracellular matrix (ECM) that can theoretically be recellularized with autologous stem or progenitor cells to yield a functional lung. Nonhuman primates (NHP) provide a highly relevant preclinical model with which to assess the feasibility of recellularized lung scaffolds for human lung transplantation. Our laboratory has successfully accomplished lung decellularization and initial stem cell inoculation of the resulting ECM scaffold in an NHP model. Decellularization of normal adult rhesus macaque lungs as well as the biology of the resulting acellular matrix have been extensively characterized. Acellular NHP matrices retained the anatomical and ultrastructural properties of native lungs with minimal effect on the content, organization, and appearance of ECM components, including collagen types I and IV, laminin, fibronectin, and sulfated glycosaminoglycans (GAG), due to decellularization. Proteomics analysis showed enrichment of ECM proteins in total tissue extracts due to the removal of cells and cellular proteins by decellularization. Cellular DNA was effectively removed after decellularization (~92% reduction), and the remaining nuclear material was found to be highly disorganized, very-low-molecular-weight fragments. Both bone marrow- and adipose-derived mesenchymal stem cells (MSC) attach to the decellularized lung matrix and can be maintained within this environment *in vitro*, suggesting that these cells may be promising candidates and useful tools for lung regeneration. Analysis of decellularized lung slice cultures to which MSC were seeded showed that the cells attached to the decellularized matrix, elongated, and proliferated in culture. Future investigations will focus on optimizing the recellularization of NHP lung scaffolds toward the goal of regenerating pulmonary tissue. Bringing this technology to eventual human clinical application will provide patients with an alternative therapeutic strategy as well as significantly reduce the demand for transplantable organs and patient wait-list time.

Introduction

Approximately 25 million people live with chronic obstructive pulmonary disease. In the United States, nearly 125,000 individuals die annually as a result of end-stage lung disease. The only current therapeutic option for these patients is lung transplantation. Unfortunately, there are a limited number of donor lungs available, and the demand for organs that meet current and future transplantation needs is staggeringly high. According to the Organ Procurement and Transplant Network (OPTN), more than 50,000 patients were placed on the lung transplantation waiting list between 1999 and 2008.[1] Nearly 1 of every 10 people on the list died while awaiting donor lungs during

This work has been previously presented in abstract form at the Stem Cells and Cell Therapies in Lung Biology and Lung Diseases Conference, Burlington, VT, 2011. Abstract no. 2.
[1]Center for Stem Cell Research and Regenerative Medicine, [2]Department of Microbiology and Immunology, Tulane University School of Medicine, New Orleans, Louisiana.
[3]RCMI Cancer Research Program, Xavier University of Louisiana, New Orleans, Louisiana.
[4]Department of Medicine, University of Vermont, Burlington, Vermont, and [5]Department of Pharmacology, Tulane University School of Medicine, New Orleans, Louisiana.

that time. As of April 18, 2012, about 16,041 patients in the United States are currently listed as lung transplant candidates. A novel means for acquiring lungs compatible for transplantation is crucial.

Whole-organ decellularization holds great promise for producing bioartificial, transplantable organs suitable for human clinical application. Scientists have reported successful decellularization and organ repopulation in the heart and liver, while a growing number of groups have reported similar success in the lung using rodent models.[2–7] Two groups recently successfully transplanted crude bioartificial rat lungs that demonstrated short-term pulmonary function *in vivo*; however, both studies utilized freshly isolated pulmonary cells from fetal or neonatal rats to repopulate the acellular rat lung matrices.[4,6,8] A more feasible option may be to utilize autologous stem or progenitor cells, and initial studies describing recellularization of rodent lungs with either embryonic stem cells (ESC) or adult bone marrow-derived mesenchymal stem cells (BMSC) have been described.[7,9] However, while offering proof of concept, murine models may not be ideal for translation into clinical studies in humans. Nonhuman primate (NHP) models offer the advantage of closely resembling the biology of humans while also allowing flexible manipulation for greater extrapolation to human use.

We describe here the successful decellularization of lungs from the rhesus macaque, a NHP, utilizing a procedure developed in our lab that has minimum impact on the lung matrix. A comprehensive spectrum of histological and protein analytical techniques were used to characterize the components of the resulting acellular matrix relative to native macaque lungs. Acellular scaffolds were effectively seeded with rhesus adult stem cells from both bone marrow and adipose tissue to study their interaction with the matrix, their applicability in recellularizing the matrix, and, ultimately, their potential for regeneration of functional pulmonary tissue to develop a bioartificial organ suitable for *in vivo* transplantation.

Materials and Methods

Generation of acellular macaque lung scaffolds

Intact heart–lung blocs were isolated during necropsy from normal rhesus macaques (*Macaca mulatta*) undergoing euthanasia at the Tulane National Primate Research Center (TNPRC). All animal procedures conformed to the requirements of the Animal Welfare Act and all animal protocols were approved by the Institutional Animal Care and Use Committee (IACUC) of the TNPRC before implementation of experimental protocols. Tissues from four male macaques aged 5.71 ± 2.73 years and three female macaques aged 3.17 ± 2.11 years were used in these studies. Immediately upon extraction, the lungs were washed in phosphate-buffered saline (PBS) containing 100 U/mL penicillin, 100 μg/mL streptomycin, and 5 mM EDTA. As soon as possible after extraction and washing, the lung vasculature was perfused via the pulmonary artery with PBS (without divalent cations) containing 50 U/mL heparin and 5 μg/mL sodium nitroprusside by gravity-driven flow at a pressure of 25–30 cm H_2O. The left atrium was lacerated to allow low resistance flow of the effluent perfusate from the pulmonary veins.

Native lung fixation was accomplished by rapidly and completely inflating the cadaveric organs with 10% neutral-buffered formalin (NBF) via intratracheal instillation using a specialized inflation apparatus that created a constant pressure of 25–30 cm H_2O for ~45 min. The formalin-inflated lungs were bathed in formalin for 24 h. The trachea was then clamped shut with a hemostat before removing the cannula that delivered the pressurized fixative. The inflation-fixed lungs were stored in 10% NBF at 4°C until samples were dissected and prepared for histology.

Lung decellularization was performed using a modification of a published protocol.[5,7] Briefly, on day 1, the lungs were washed by intratracheal inflation with deionized (DI) water solution (DI water, 500 U/mL penicillin, and 500 μg/mL streptomycin). The lungs were allowed to expel the fluid by natural recoil and the washing step was repeated five times. The pulmonary vasculature was then perfused via cannulation of the pulmonary artery with the DI water solution five times to remove any remaining blood. Triton X-100 solution (0.1% Triton X-100, 500 U/mL penicillin, and 500 μg/mL streptomycin) was then instilled into the airway and throughout the vasculature as before. The lungs were incubated at 4°C for 24 h bathed in the Triton X-100 solution. On day 2, the lungs were washed with DI water solution as described previously followed by airway instillation, vasculature perfusion, exterior bathing, and incubation with deoxycholate solution (2% sodium deoxycholate [SDC], 100 U/mL penicillin, and 100 μg/mL streptomycin) at 4°C for 24 h. On day 3, the lungs were removed from deoxycholate solution and washed as before with DI water solution. Hypertonic saline (1 M NaCl, 500 U/mL penicillin, and 500 μg/mL streptomycin) was instilled and perfused, and the lungs were bathed in the NaCl solution at room temperature for 1 h. NaCl solution was removed by DI water washes, and a solution of bovine pancreatic DNase (30 μg/mL DNase, 1.3 mM $MgSO_4$, 2 mM $CaCl_2$, 500 U/mL penicillin, and 500 μg/mL streptomycin) was instilled and perfused as before. The lungs were incubated at room temperature for 1 h bathed in DNase solution followed by five washes with PBS solution (PBS without Ca^{2+}/Mg^{2+}, 500 U/mL penicillin, 500 μg/mL streptomycin, and 1.25 μg/mL amphotericin B). De-cellularized lungs were then stored in PBS solution at 4°C.

Histological characterization

Both native and acellular macaque lung tissues were fixed and prepared for histological analysis as follows. For inflation-fixation, the whole native lungs were attached to a gravity-driven inflation apparatus composed of an elevated reservoir of 10% NBF, which drained to an intermediate reservoir that created a pressure head 25–30 cm H_2O above the lungs. Flow of formalin fixative into the cannulated lungs was initiated by opening control valves along the apparatus flow path. The lungs were inflated under a constant pressure of 25–30 cm H_2O while bathed in NBF for 1 h. Fixed native lungs were then stored in fresh NBF at 4°C until use in histological assays. Blocks of tissue of 2–3 cm^3 were cut from inflation-fixed native macaque lung and embedded in paraffin. Single lobes of de-cellularized macaque lung were fixed by inflation as described above followed by dissection into 2–3-cm^3 blocks and paraffin embedding. Native and acellular tissues were cut into 5-μm sections and mounted on glass microscope slides. Hematoxylin and eosin (H&E), Gomori

trichrome, modified Movat's pentachrome, and alcian blue staining were performed by the Center for Stem Cell Research and Regenerative Medicine Histology Core Facility using standard protocols. Stained tissue sections were scanned with the Aperio ScanScope (Aperio) at an initial magnification of 40×, and images were visualized and captured using the Aperio ImageScope program. Comparisons were made using samples from age- and gender-matched animals.

Threshold and mean linear intercept analyses

Twenty random images of equal magnification (400×) from H&E-stained native and de-cellularized lung tissue specimens were captured via ImageScope. Image analyses were performed with ImageJ. For threshold analysis (percent parenchyma), the images were digitally adjusted to remove background and increase the contrast between the tissue (alveoli) and the airspace. The RGB images were converted to 8-bit, and threshold determinations were used to digitally highlight all the parenchymal tissue while leaving the airspace untouched. Finally, the percent of highlighted pixels (tissue) was calculated relative to total area of the field. Data were recorded as percent parenchyma relative to airspace.[7]

The same 20 images from native and de-cellularized lung H&E staining were used to calculate mean linear intercept (MLI), the probability of a random line of fixed length encountering parenchymal tissue when traveling through the lung. MLI was determined by overlaying a grid of known area randomly onto the H&E images using ImageJ. Image scale was set according to the scale bar. Then, using the plugin "Grid," a randomly offset grid of known area was superimposed on the image. The number of times each horizontal line intercepted an alveolar septum was counted, and MLI was calculated by dividing the number of intercepts per line by the length of the line; therefore, data are reported as intercepts per micrometer.

Immunohistochemistry of matrix proteins

Immunohistochemistry (IHC) was performed on native and acellular macaque lung sections using mouse monoclonal primary antibodies (IgG isotype) for collagen types I and IV, fibronectin, laminin, and vitronectin (Millipore). All stains used the secondary antibody AlexaFluor 568 goat anti-mouse IgG (H + L) from Invitrogen. Secondary antibody-only and IgG isotype controls used Tris-buffered saline (TBS) without primary antibody or normal mouse IgG isotype antibody for initial incubations, respectively, followed by staining with the same AlexaFluor 568 secondary antibody. After extensive washing with TBS, all sections were stained with 0.3 mM DAPI for 5 min followed by washing with TBS, air-drying, and coverslip mounting with Prolong Gold Antifade Reagent (Molecular Probes). Images were captured by standard fluorescent microscopy using the Olympus IX71 inverted microscope fitted with an Olympus DP70 digital camera.

Proteomics

Tissue samples of approximately equal size (~3 cm^3) were dissected from the upper right lobe of native and de-cellularized macaque lungs. The tissue was snap-frozen in liquid nitrogen and ground to a fine powder using a prechilled mortar and pestle. The powdered tissue homogenate was suspended in RIPA buffer containing 1× protease inhibitor cocktail (Thermo Scientific). The lysates were incubated overnight at 4°C with gentle rotation. The next day, the lysates were cleared by centrifugation at 14,000 *g* for 10 min at 4°C. Supernatants were collected, bicinchoninic acid assay (BCA) assay (Pierce) was used to determine the protein concentration in native and de-cellularized lung lysates, and samples were stored at −80°C. Analysis of protein lysates was performed by the RCMI Core facility at Xavier University of Louisiana in New Orleans. Equal amounts (100 μg per sample) of native and de-cellularized lung tissue were processed for the LC-MS/MS analysis. Additional experimental details are included in Supplementary Methods (Supplementary Data are available online at www.liebertpub.com/tea) for trypsin digestion, desalination of fractionated samples, LC-MS/MS Analysis on LTQ-Orbitrap, and IPI.Human.fasta.v3.77 database search. The results of the database search were sorted according to the number of peptides identified (greatest to least) and tabulated to visualize the prevalence of extracellular matrix (ECM) proteins between the samples. All peptides were categorized as follows: cytosol, membrane, cytoskeleton, ECM, nucleus, and secreted/non-ECM. The percentage occupied by each group was determined by dividing the number of peptides by the total number of peptides identified per sample. Some totals exceed 100% because some peptides occupy more than one category.

Western blot

Protein lysates from native and de-cellularized lung were prepared by homogenizing tissue in RIPA buffer containing 1× HALT protease inhibitor cocktail (Thermo Scientific) using a Dounce homogenizer. Twenty-five micrograms of protein from native and de-cellularized lung lysates was loaded to 4%–12% NuPage Bis-Tris gels (Invitrogen) for electrophoresis. See Supplementary Methods for Western blotting conditions.

GAG quantification

Sulfated GAG were quantified by a modification of a previously described method.[10,11] Briefly, equal tissue wet weight (2 g) biopsies were excised from native and decellularized macaque lungs, lyophilized, and digested in 100 mM K_2HPO_4 (pH 8.0) containing 50 μg/mL proteinase K at 56°C overnight. After digestion, the lysates were heat-inactivated at 90°C for 10 min and cleared twice by centrifugation at 20,000 *g* for 10 min. Cleared lysates were filtered through Ultra-free 30,000 NMWL filters (Millipore) by centrifugation at 20,000 *g* for 30 min to remove cell debris and extruded DNA. Filtrates were collected and assayed for protein concentration by BCA (Pierce). GAG were quantified by colorimetric assay by mixing 10 μL of cleared tissue lysates with 200 μL of 1-,9-dimethylmethylene blue (DMMB) working solution (16 g/L DMMB, 3.04 g/L glycine, and 2.37 g/L NaCl, pH 3.0). Absorbance at 525 nm was read immediately. Absorbance values of samples were compared to those of a standard curve of chondroitin sulfate prepared in the same buffer and processed in parallel with the tissue lysates. Tissue concentrations of GAG (μg/mL) were normalized to extracted protein concentration (μg/mL) for each sample.

Genomic DNA isolation and quantification

Total genomic DNA (gDNA) was isolated from native and decellularized macaque lung biopsies using the DNeasy kit from Qiagen according to manufacturer protocol. Briefly, random biopsies were taken from native and acellular lung using sterile surgical tools. The tissue fragments were weighed and dissected into 25-mg pieces. The tissue pieces were minced with sterile razor blades before processing with the Qiagen kit. All samples were processed in parallel and resulted in identical volumes of gDNA-containing solutions. The resulting gDNA was quantified using a NanoDrop spectrophotometer (Thermo Scientific). The mean values for total gDNA yield were determined for each native and decellularized lung tissue sample and differences were assessed by Student's *t*-test. The DNA recovered from decellularized lung samples was precipitated using 0.1× volumes of 3 M sodium acetate and 2.5× volumes of 100% ethanol, pelleted, washed with 70% ethanol, pelleted again, and resuspended in 25 μL of nuclease-free water. Five hundred nanograms of gDNA from each native and decellularized sample was loaded into a 0.8% Ultrapure agarose gel (Invitrogen). The samples were subjected to electrophoresis at 80V for ~45 min before imaging the gel using the ImageQuant LAS 4000 system (GE).

Seeding the acellular matrix with stem cells

Rhesus primary BMSC and adipose-derived mesenchymal stem cells (ASC) were harvested, cultured, and characterized as previously described.[12–14] (See Supplementary Methods for details on MSC isolation and culture.)

Both BMSC and ASC were cultured in complete culture medium (CCM) composed of α-minimum essential medium supplemented with 16.4% fetal bovine serum, 4 mM L-glutamine, 100 U/mL penicillin/streptomycin, and 250 ng/mL amphotericin B at 37°C and 5% CO_2. Cells used in these experiments were passage 7 or below and were not allowed to reach confluence of greater than 70%. The cells were lifted from the culture plates with trypsin, pelleted, and resuspended to 1.5×10^6 cells/mL in 25 mL of CCM. The cell suspensions was mixed at a 1:1 ratio with liquefied 2% low-melting-point agarose (1% final) at 37°C. The mixtures were instilled into single lower lobes of decellularized macaque lungs that had been washed three times with PBS containing 100 U/mL penicillin, 100 μg/mL streptomycin, and 250 ng/mL amphotericin B and then washed three times with CCM warmed to 37°C. The cell–agarose mixtures were instilled into the primary bronchioles using 60-cc catheter-tip syringes fitted with 1-cc pipette tips. After inflating the lobes with the individual cell suspensions, the seeded scaffolds were placed in ice-cold PBS with antibiotics/antimycotics and incubated at 4°C for 15 min to solidify the agarose. Once solid, the seeded tissues were cut into ~1-mm slices using sterile scalpels, and the slices were then cultured in six-well plates containing CCM. Each day of culture, the medium was changed, and the slices were inverted to ensure even nutrient and oxygen availability. After 7 days in culture, the slices were washed three times with PBS and then fixed in 10% NBF for 30 min at room temperature. The fixed slices were embedded in paraffin, sectioned at 5 μm, and mounted onto glass slides. The sections were stained with H&E and scanned using the Aperio ScanScope. Images were acquired using the ImageScope program.[7]

Proliferation and apoptosis. To examine the occurrence of proliferation and/or apoptosis of stem cells seeded into the decellularized macaque lung, IHC was performed on BMSC- and ASC-seeded macaque lung scaffold sections for the cell proliferation marker Ki67 along with TUNEL staining for apoptosis. Details regarding Ki67 and TUNEL staining can be found in Supplementary Methods. To determine the percentage of cells that stained positive for Ki67 or TUNEL, 10 random fields for each were imaged at a magnification of 5× and analyzed using ImageJ. Briefly, total cells per field were determined by first converting DAPI images to 8-bit and inverting the resulting grayscale image (nuclei appear black on white background). Automatic threshold and watershed segmentation were applied to the image. Particle count analysis was used to count the number of nuclei per field. Cells staining positive for Ki67 or TUNEL were counted by eye, and the values for each were divided by the total number of cells determined by particle count as above.

Cell–ECM interactions (IHC). To assess the interaction of stem cells seeded into the acellular macaque lung scaffolds with the native ECM proteins of the scaffold, IHC was performed on the BMSC- and ASC-seeded 24-h and 7-day slice cultures. Briefly, the slices were rinsed with PBS and fixed in 10% NBF for 16–20 h at 4°C before processing and paraffin embedding. Sections (4 μm) were deparaffinized by consecutive 3-min incubations starting with xylene, then to ethanol, followed by rehydration in water. IHC was performed using purified mouse anti-fibronectin (BD), laminin (Abcam), collagen I (Abcam), and collagen IV (Abcam) primary antibodies. Secondary antibodies used were AlexaFluor 568 goat anti-rabbit IgG (H + L) (Invitrogen) and AlexaFluor 568 $F(ab')_2$ fragment of goat anti-mouse IgG (H + L) (Invitrogen). After staining, tissue was submerged in Aqua Polymount (Lerner Laboratories) and cover slips were added and sealed with nail polish. Staining was analyzed using an Olympus BX50 Light Microscope fitted with a QImaging Retiga 2000R digital camera.

Cell–ECM binding array. See Supplementary Methods.

Statistical analyses

Statistical comparisons for Western blot equal loading and DNA quantification were analyzed using Student's *t*-test. *p*-Values of <0.05 were considered to be statistically significant. Cell–ECM binding array data were compared by two-factor analysis of variance (ANOVA) with replication for profiling the binding of BMSC versus ASC across various ECM protein ($\alpha = 0.05$) groups followed by Bonferroni *post hoc* analysis for BMSC versus ASC binding to specific ECM proteins. Binding of BMSC and ASC to various ECM proteins was individually analyzed by single-factor ANOVA ($\alpha = 0.05$) with Bonferroni *post hoc* analysis between ECM groups ($\alpha = 0.0018$).

Results

Macaque lungs are successfully decellularized by the Triton X-100/SDC method

Whole lungs from euthanized rhesus macaques were subjected to inflation-fixation (Supplementary Fig. S1;

Supplementary data available at www.libertpub.com/tea) or detergent-mediated decellularization (Fig. 1). Supplementary Figure S1A shows an example of cadaveric lungs, *ex vivo* (deflated), in preparation for inflation fixation or decellularization. Whole lungs were efficiently inflation-fixed and stored in formalin (Supplementary Fig. S1C, D). After sequential instillation of decellularization reagents and extensive washing of lungs from age- and gender-matched animals, the resulting acellular matrix scaffolds retained the shape of the native lungs and were stored intact in PBS containing 500 U/mL penicillin, 500 μg/mL streptomycin, and 1.25 μg/mL amphotericin B (Fig. 1B, C).

Detergent treatment removes cells while leaving ECM components of the lungs intact

Structural components, including large blood vessels, capillaries, large and small bronchioles, respiratory bronchioles, and alveolar sacs and were identifiable by H&E stain and had little variation from the normal architecture in native lungs (Fig. 2A). Efficiency of decellularization was noted by the absence of darkly stained nuclei in H&E (Fig. 2B, F),

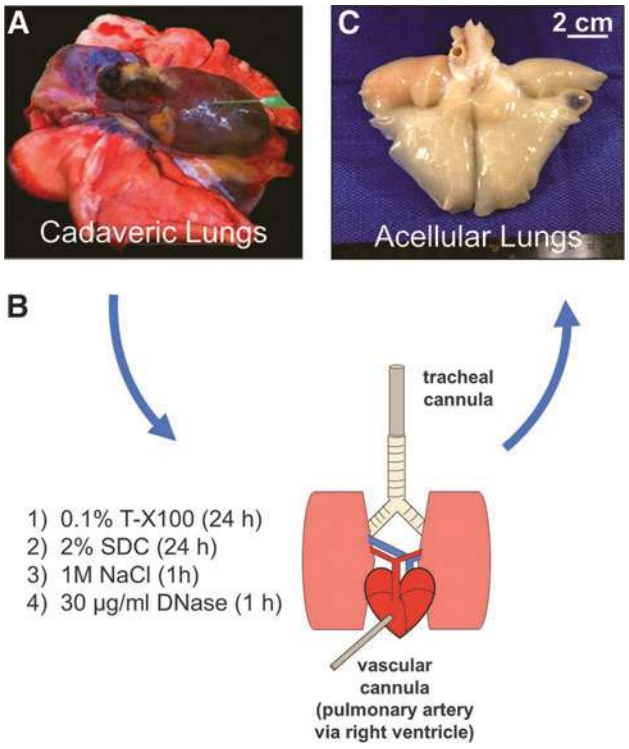

FIG. 1. Decellularized macaque lungs are efficiently generated using the Triton/SDC method. **(A)** Cadaveric lungs (pictured collapsed, *ex vivo*) from rhesus macaques undergoing euthanasia were decellularized by the Triton X-100/SDC method. **(B)** For decellularization, the cadaveric lungs were subjected to sequential instillation of detergents, hypertonic saline, and DNase into the airway via the trachea and through the vasculature via the right ventricle and pulmonary artery over a period of 3 days. **(C)** The resulting decellularized lungs retain the ultrastructural and microanatomical features of native lungs including maintenance of large air-conducting passages, blood vessels, and lung parenchyma. SDC, sodium deoxycholate. Color images available online at www.liebertpub.com/tea

Gomori (Fig. 2C, G), and Movat's stains (Fig. 2D, H). The eosinophilic connective and ECM structures are still visible after decellularization (Fig. 2F). Collagen fibers stained bright green with Gomori trichrome, and bundles of collagen were well preserved in the acellular matrix (Fig. 2G). With Movat's stain, darkly staining elastic tissue was seen in alveolar septae (Fig. 2D, H, gray arrows), endothelial matrices (not shown), and at the axes of respiratory bronchioles (black arrows). Some loss of elastic fibers was noticed by histological examination after decellularization. Alcian blue staining for GAG showed no appreciable reduction in the content of GAG after decellularization; however, the organizational morphology of GAG in the acellular matrix appeared ragged compared to native lung (Fig. 2E, I).

The images from H&E staining were analyzed for determination of field threshold area (Supplementary Fig. S2). Native lung parenchyma constituted 24.3% ± 4.3% of the field area at this magnification, while acellular matrix parenchyma constituted a similar field area of 24.4% ± 3.3% (Fig. 2J). Decellularized lung had a slightly but significantly smaller MLI than native lung ($p < 0.0001$) with 0.012 ± 0.002 intercepts/μm versus 0.019 ± 0.003 intercepts/μm, respectively, signifying a small increase in alveolar diameter of acellular matrix relative to that of native lung (Fig. 2K).

IHC revealed the *in situ* parenchymal content of ECM proteins. As seen in Figure 3, the abundance, orientation, and condition of collagen type I (Fig. 3A, B), collagen type IV (Fig. 3C, D), and laminin (Fig 3E, F) were virtually unaffected by decellularization; however, fibronectin appeared to take on a ragged, moth-eaten appearance in the acellular matrix relative to native lung (Fig. 3G, H). DAPI staining (Fig. 3 insets) showed multiple nuclei present in the native lung parenchyma but not in that of decellularized lung. Secondary antibody-only and nonspecific IgG isotype controls validated specificity of staining (Fig. 3I, L).

Protein analyses revealed an enriched ECM protein profile for acellular macaque lung scaffolds

Proteomics analysis returned 1061 peptides from native lung lysate samples and 157 peptides from de-cellularized lung lysate samples. Of those peptides, 812 and 138, respectively, matched known, identifiable proteins. Table 1 lists the top 10 peptide matches (sorted most-to-least peptides detected) followed by all other ECM-related proteins (below dotted line) and their position according to sort. Overall, ECM proteins were enriched >10-fold from 2.1% of total protein matches in native lung to 24.6% in de-cellularized lung (Fig. 4A). Soluble (cytoplasmic) proteins were reduced from 57.3% of identified native lung peptides to 20.3% of de-cellularized lung peptides. Proteins in all other cellular compartment categories (membrane, cytoskeleton, nucleus, and secreted/non-ECM) changed less than twofold when measured as a percentage of identified peptides in each sample.

Using actin as a representative cytoplasmic protein and fibronectin as a representative ECM protein, we performed Western blot to detect these proteins in native and decellularized lung protein lysates (Fig. 4B). Using 25 μg of total protein from each native and decellularized lysate, immunoblots demonstrated robust presence of actin in native but not decellularized lung, suggesting removal of cytoplasmic protein during decellularization. High-molecular-weight fibronectin splice

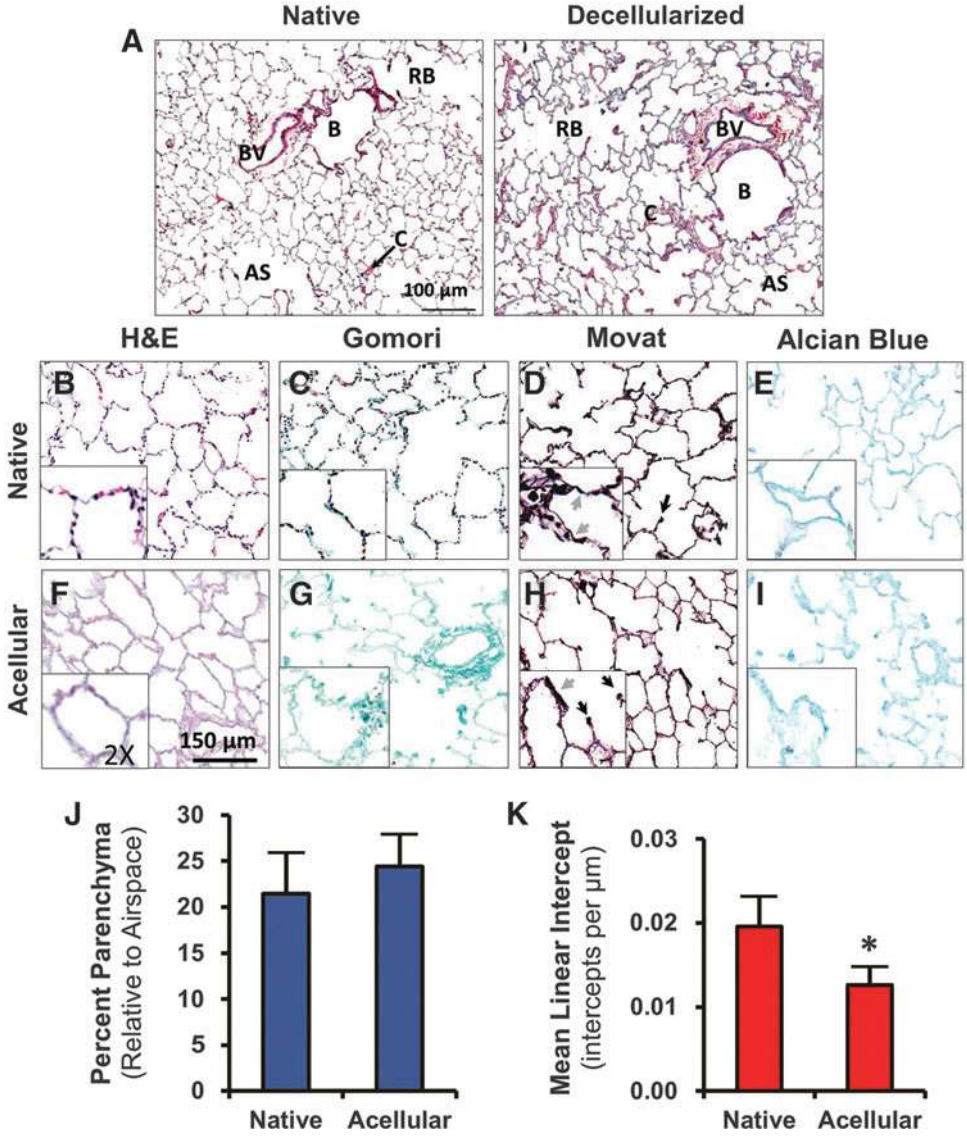

FIG. 2. Decellularized macaque lungs retain the ultrastructural and microanatomical features of native lungs. **(A)** H&E stain demonstrates a similar histological appearance of bronchioles (B), respiratory bronchioles (RB), blood vessels (BV), alveolar sacs (AS), and capillaries (C) in both native and decellularized lung. **(B–I)** Native and decellularized macaque lungs were stained with H&E **(B, F)**, Gomori's trichrome **(C, G)**, and modified Movat's pentachrome **(D, H)**, to examine various histological features. Efficiency of decellularization is evident from the lack of darkly staining nuclei in H&E, Gomori, and Movat's stains. Gomori shows that preserved collagen (green) remains in abundance after decellularization. Movat's stain shows the presence of septal elastic tissue (gray arrows) and axial elastic tissue (black arrows) in both native and decellularized lung; there is visibly less elastic tissue in the decellularized lung as noticed by this stain. **(E, I)** Alcian blue stain was used to observe the content of GAG in native and decellularized lungs. GAG are preserved through decellularization but take on a ragged appearance histologically. **(J)** Native and decellularized lung have similar parenchyma-to-airspace area, but **(K)** acellular lung has a slightly but significantly lower MLI than native lung ($p < 0.0001$), suggesting that decellularization produces alveoli that are of slightly larger diameter than native lungs. Insets represent a 2× enlarged portion of each field to show fine details. The asterisk indicates $p < 0.05$ by Student's *t*–test. H&E, hematoxylin and eosin; MLI, mean linear intercept; GAG, glycosaminoglycans. Color images available online at www.liebertpub.com/tea

variants were detected in native lung. By contrast, decellularized lungs showed increased (enriched) amounts of fibronectin immunoreactive material, but the bands were smudged throughout the lane, indicating some degree of protein degradation consistent with the previous histological results using IHC, which showed a moth-eaten appearance of fibronectin.

Sulfated GAG content is retained in decellularized lungs relative to native lungs (Fig. 4C). Since it is impossible to assay total GAG in whole macaque lungs, random biopsies of similar size were used. Consistent with histological findings, a biochemical quantification of sulfated GAG using DMMB dye and a chondroitin sulfate standard curve showed that, when normalized to extracted protein content, the concentration of GAG in decellularized lungs was $1.39 \times 10^{-2} \pm 0.660 \times 10^{-2}$ μg/mL per μg/mL of total extracted protein. Native lungs assayed in the same manner

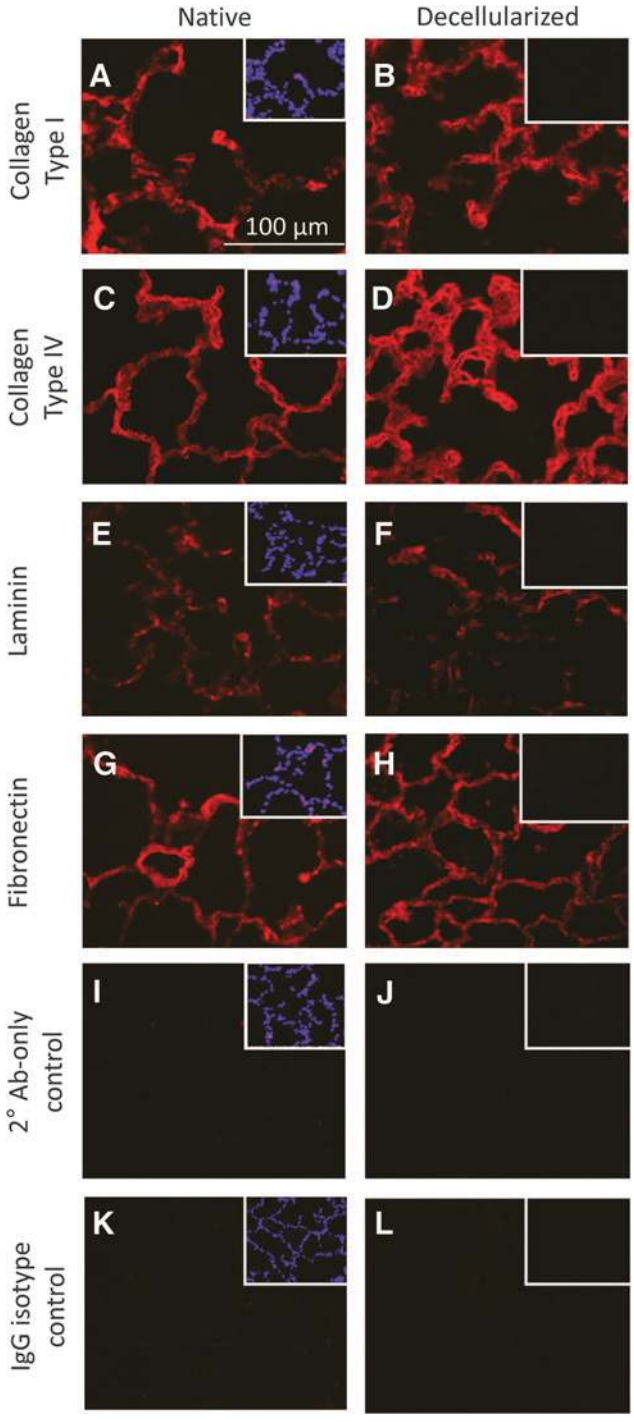

FIG. 3. IHC reveals maintenance of ECM proteins after decellularization. **(A–D)** Collagen type I and collagen type IV are retained after decellularization and appear minimally affected by the decellularization process. **(E–H)** Laminin and fibronectin are retained in equal abundance in decellularized lung; however, the organization of these proteins in the acellular scaffold appears ragged and moth-eaten. **(I–L)** Secondary antibody-only and IgG isotype controls for staining show no appreciable fluorescence in native or decellularized lung tissue. Insets in all panels show DAPI staining of the field; bright nuclear-specific staining can be observed in native lungs but not in decellularized lungs. IHC, immunohistochemistry. Color images available online at www.liebertpub.com/tea

yielded $1.03\times10^{-2}\pm0.334\times10^{-2}$ μg/mL sulfated GAG per μg/mL extracted protein. No statistical difference existed between these values for native and decellularized lung samples ($p=0.187$, $n=8$).

DNA is efficiently removed during decellularization

The amount of gDNA in native versus decellularized lung was compared to analyze the efficiency of DNA removal by detergent-mediated decellularization. Quantification of total DNA recovery showed significantly less ($p=0.006$) DNA recovered from decellularized lung relative to that from native lung (Fig. 4D). Gel electrophoresis of recovered DNA showed high-molecular-weight bands for native lung while DNA from decellularized lung was only faintly detected with the majority appearing as low-molecular-weight degradation products (Fig. 4E).

BMSC and ASC adhere to the acellular macaque lung matrix, elongate along the alveolar septae, and proliferate in vitro

Rhesus BMSC and ASC each suspended in a 1:1 mix of cell culture medium and liquefied low melting-point agarose (37°C) were instilled into separate single lobes of acellular lungs via the secondary bronchi (Supplementary Fig. S3A). The agarose/cell mixture–containing lobes were solidified at 4°C for 15 min, and the cell-seeded lobes were cut into 1-mm-thick slices and cultured in CCM (Supplementary Fig. S3B). Twenty-four hours later, cells could be observed attaching to and spreading on the alveolar septal matrix (Fig. 5A, E), and after 7 days, the cells remained attached and retained the elongated phenotype (Fig. 5B, F). No free-floating (unattached) cells were noted within the alveolar spaces upon histological assessment of the slice cultures. Higher magnification (30×) views of BMSC and ASC after 7 days of culture showed dark nuclei and lighter (eosinophilic) cytoplasm (Fig. 5C, G, arrows). In addition to adherence to distal lung parenchyma structures, such as respiratory bronchioles and alveoli, both BMSC and ASC also adhere to the internal surface of larger air-conducting passages, that is, secondary and tertiary bronchioles (Fig. 5D, H).

Ki67 and TUNEL staining were used to assess whether the cells inoculated into the decellularized macaque lung matrix were proliferating or undergoing apoptosis, respectively. Both Ki67- and TUNEL-positive cells were observed in both ASC- and BMSC-seeded 3D matrices from slice cultures (Fig. 6 inset). Of the cells inoculated into the decellularized matrix, 25.7%±12.9% of ASC and 19.8%±13.1% of BMSC showed signs of proliferation after 7 days in culture, while only 4.0%±1.5% of ASC and 7.4%±4.4% of BMSC were actively undergoing apoptosis (Fig. 6).

The cell-seeded matrices were analyzed by IHC for the binding of the cells to areas of the matrix scaffold that are rich in particular ECM proteins. A subjective comparative analysis of these images suggested that association with collagen type I is marginal at 24 h for both cell types; however, at 7 days, the ASC showed a more distinct association with areas identified as being dense in collagen type I and displayed a cell body-like silhouette of positive staining consistent with the observations of Daly *et al.* (Fig. 7A–D). White arrows in Figure 7 point to the cells where this phenomenon is most robust. BMSC seemed to be associated with

Table 1. Proteomics Database Search Results Sorted for Frequency of Peptides (Greatest to Least) and Rank of Extracellular Matrix Proteins Identified

Native macaque lung			*Decellularized macaque lung*		
Rank	*No. of peptides*	*Description*	*Rank*	*No. of peptides*	*Description*
1	80	Neuroblast differentiation-associated protein AHNAK	1	18	Isoform 1 of Annexin A2
2	52	Filamin A, alpha Ing=2607	2	18	Isoform 6 of myoferlin
3	52	Talin-1	**3**	**14**	**Fibrillin-1**
4	51	Isoform 2 of spectrin alpha chain, brain	**4**	**11**	**Collagen alpha-3(VI) chain isoform 4 precursor**
5	50	Isoform 1 of myosin-9	5	8	Annexin A6
6	34	Isoform long of spectrin beta chain, brain 1	6	8	cDNA FLJ90527 fis, clone NT2RP4004167, highly similar to 5′-nucleotidase
7	30	Isoform 2 of Clathrin heavy chain 1	7	8	Isoform 1 of myosin-10
8	30	Myosin-11 isoform SM2A	8	8	Isoform beta-1B of integrin beta-1
9	27	Isoform 1 of vinculin	9	8	Keratin, type II cytoskeletal 1
10	26	Cytoplasmic dynein 1 heavy chain 1	**10**	**8**	**Laminin subunit gamma-1**
141	**7**	**Lumican**	**15**	**7**	**Basement membrane-specific heparin sulfate proteoglycan crore protein variant Ing=4374**
200	**5**	**Collagen alpha-3(VI) chain isoform 4 precursor**	**17**	**7**	**Laminin subunit alpha-3 isoform 3**
264	**4**	**Collagen alpha-1(VI) chain**	**24**	**5**	**Chondroadherin**
382	**3**	**Isoform 2 of Collagen alpha-1(XIV) chain**	**26**	**4**	**Collagen alpha-2(IV) chain**
410	**3**	**Prolargin**	**31**	**4**	**Iosform A of Decorin**
486	**2**	**cDNA FLJ35535 fis, clone SPLEN2002419, highly similar to EGF-containing fibulin-like extracellular matrix protein 1**	**33**	**4**	**Laminin subunit alpha-5**
527	**2**	**Fibulin-5**	**34**	**4**	**Laminin subunit beta-2**
573	**2**	**Isoform A of fibulin-1**	**43**	**3**	**cDNA FLJ60269, highly similar to *Homo sapiens* nephronectin (NPNT), mRNA**
769	**1**	**Collagen alpha-2(IV) chain**	**45**	**3**	**Collagen alpha-1(VI) chain**
861	**1**	**Isoform 2C2A′ of collagen alpha-2(VI) chain**	**46**	**3**	**Collagen alpha-2(I) chain**
			48	**3**	**Fibulin-5**
			62	**2**	**cDNA FLJ51266, highly similar to vitronectin**
			65	**2**	**Isoform 1 of collagen alpha-6(VI) chain**
			94	**1**	**cDNA FLJ53292, highly similar to *Homo sapiens* fibronectin 1 (FN1), transcript variant 5, mRNA Ing=1014**
			99	**1**	**cDNA FLJ61309, highly similar to Laminin beta-3 chain**
			101	**1**	**Collagen alpha-4(IV) chain**
			116	**1**	**Isoform 1 of collagen alpha-1(II) chain**
			122	**1**	**Isoform 2 of collagen alpha-3(IV) chain**
			127	**1**	**Isoform 3 of aggrecan core protein**
			131	**1**	**Isoform long of laminin subunit gamma-2**

Entries in bold represent peptides identified as being derived from the extracellular matrix.

laminin-dense areas by day 7 with cell body-like positive staining but did not initially show any particular preference for this protein at 24 h postinoculation (Fig. 7I, J). At 24 h, ASC showed close association with laminin-dense areas, and this association was reduced by day 7 (Fig. 7K, L). No change in ECM-specific association or cell body-like staining was evident for the ubiquitous collagen IV (Fig. 7E–H) or the predominantly vascular matrix-associated fibronectin (Fig. 7M–P) at 24 h or at 7 days after seeding of either cell type. Secondary antibody-only and IgG isotype control stains confirmed specificity of staining (Fig. 7Q–S).

The initial binding affinity of both rhesus ASC and BMSC to individual ECM proteins *in vitro* was evaluated by ECM binding array according to the number of cells that attach to individual ECM proteins during a fixed amount of time (represented by relative fluorescence units). Cell attachment to collagen type I, collagen type II, collagen type IV, fibronectin, laminin, tenascin, and vitronectin was tested. Bovine

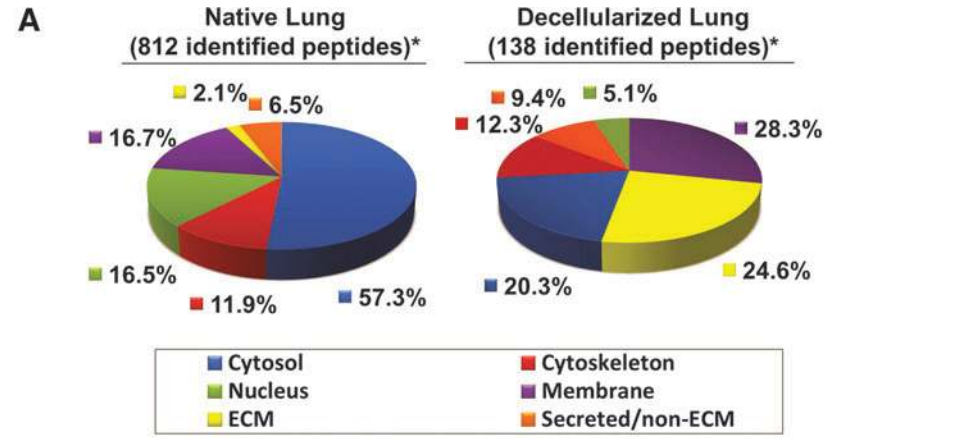

FIG. 4. Protein and DNA macromolecular profiles of native and decellularized macaque lung show enrichment of ECM proteins and depletion of DNA after decellularization. **(A)** Proteomics analysis of equal amounts (i.e., protein content) of tissue lysate from native and decellularized macaque lung demonstrates the efficient removal of cellular material from the native scaffold such that ECM peptides are enriched in decellularized lung lysates, while cytoplasmic proteins are reduced. **(B)** Actin, a cytoplasmic protein, is detected in native lung protein lysates, but is not detected in decellularized lung lysates. Fibronectin splice variants are detected in native lung lysates, and while there is enriched fibronectin immunoreactive material in decellularized lung samples, it appears to be degraded by decellularization. **(C)** Quantification of remaining GAG in decellularized lungs reveals that the total protein concentration-normalized values are similar to those of native lung ($p = 0.187$, $n = 8$). **(D)** gDNA is isolated in abundance from native lung tissue; however, the amount of gDNA from an equal tissue mass of decellularized lung is significantly less ($p = 0.006$). **(E)** Gel electrophoresis analysis of 500 ng of DNA recovered from native and decellularized lung show a high-molecular-weight band corresponding to gDNA in native lung, but this band is only faintly visible in decellularized lung samples of equal load. Moreover, the DNA recovered from decellularized lung shows low-molecular-weight degradation products. The asterisk indicates $p < 0.05$ by Student's *t*-test. MW, molecular weight; Kb, kilobases; N, native; D, decellularized; ECM, extracellular matrix; gDNA, genomic DNA. Color images available online at www.liebertpub.com/tea

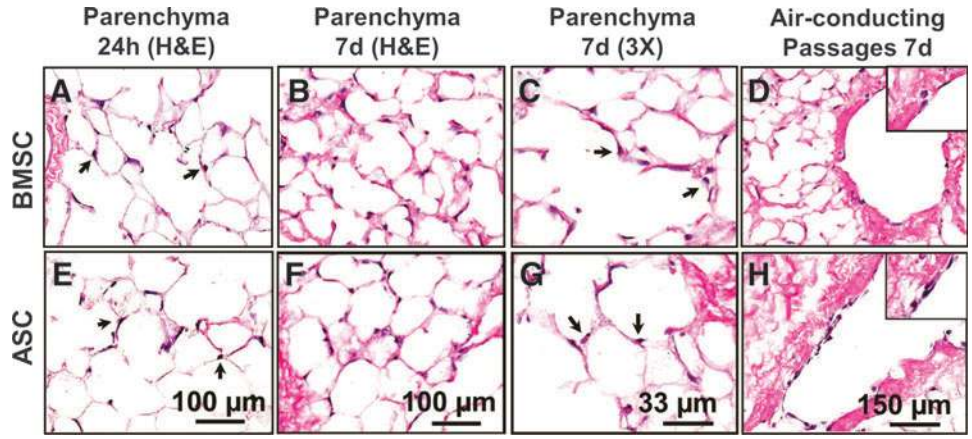

FIG. 5. Initial seeding of rhesus BMSC and ASC within the acellular lung matrix shows adhesion and elongation in culture. **(A–H)** Rhesus BMSC and ASC seeded into decellularized macaque lung scaffolds attach to the matrix and persist in culture. **(A, E)** After 24 h (24h), cells were observed attaching to the matrix by H&E stain (arrows). **(B, F)** At 7 days (7d), cells persisted in the matrix and maintained an elongated phenotype. **(C, G)** High magnification (30×) images of H&E stained sections from 7d samples showed dark (hematoxylin-stained) nuclei and lighter (eosinophilic) cytoplasmic projections (arrows). **(D, H)** In addition to adherence to the alveolar septal matrix, both BMSC and ASC adhere to air-conducting passages. Images acquired at 100× or 300× magnification as indicated; insets represent 300× magnification. BMSC, bone marrow-derived mesenchymal stem cell; ASC, adipose-derived mesenchymal stem cells. Color images available online at www.liebertpub.com/tea

serum albumin served as a negative control. BMSC and ASC had significantly different adhesion profiles among all ECM proteins as tested by ANOVA ($p<0.0001$) (Supplementary Fig. S4 and Supplementary Table S1A). Supplementary Table S1B and C lists *p*-values for comparisons of BMSC and ASC adhesion to the ECM proteins listed in Supplementary Figure S4. BMSC showed significant variation in the number of adherent cells among ECM groups by single-factor ANOVA ($p<0.0001$) (Supplementary Table S1B). *Post hoc* analysis with Bonferroni correction ($\alpha=0.0018$) shows significantly different binding of the BMSC to vitronectin and collagen type II only. Conversely, there were no significant differences in ASC binding among the ECM groups by ANOVA ($p=0.2144$), nor were there any significant differences for any combinations of ECM groups aside from the negative control after *post hoc* analysis with Bonferroni correction (Supplementary Table S1C).

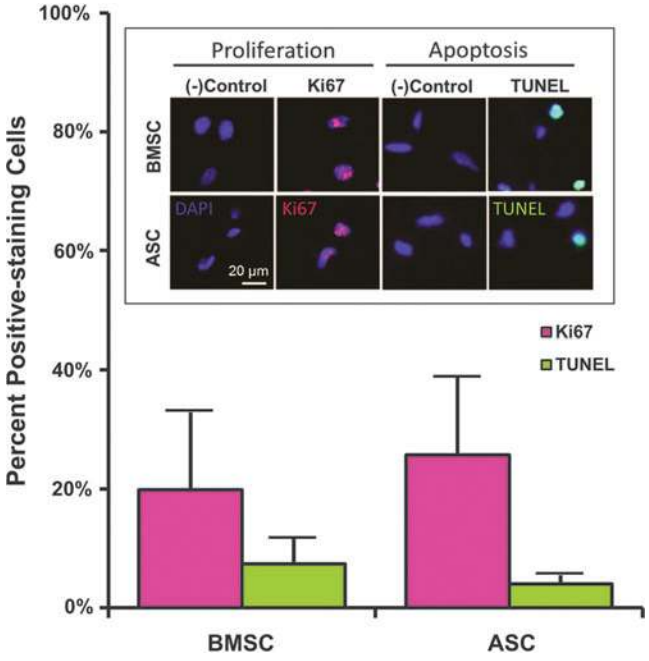

FIG. 6. Rhesus BMSC and ASC proliferate within the acellular lung matrix. Both proliferating and apoptotic cells were observed after 7 days' culture of BMSC and ASC in the decellularized macaque lung matrix as determined by Ki67 and TUNEL staining, respectively (inset). Approximately 20.0% and 25.7% of BMSC and ASC, respectively, show Ki67-positive staining (proliferation) after 7 days in 3D culture, while only 7.4% and 4.0%, respectively, are positive for TUNEL (apoptosis) at 7 days after cell inoculation. Color images available online at www.liebertpub.com/tea

Discussion

This is the first demonstration of efficient whole-lung decellularization in a nonrodent, large animal model—the NHP, rhesus macaque. In general, primates, including humans, share highly conserved anatomical, physiological, and morphological homology. The rhesus macaque shares ~93% sequence homology with humans at the genome level and has a similar pattern of lung development and growth as humans.[15,16] Therefore, macaques are an excellent preclinical model in which to investigate lung bioengineering before human use. However, in order to use decellularized lung scaffolds as a basis for regenerative medicine, the ECM must be minimally perturbed by the process of decellularization. In addition, cell–matrix interaction is crucial during organogenesis and wound healing; therefore, it is presumed that successful re-establishment of functional tissue using bioartificial means must closely recapitulate these natural processes. Several groups, including ours, have demonstrated that the Triton/SDC method of decellularization in rodent lungs produces acellular scaffolds that maintain ECM integrity while efficiently eliminating cellular material.[5,7] Notably, mouse lungs decellularized with Triton/SDC support robust proliferation and long-term (4-week) growth after intratracheal inoculation of bone marrow-derived MSC.[7]

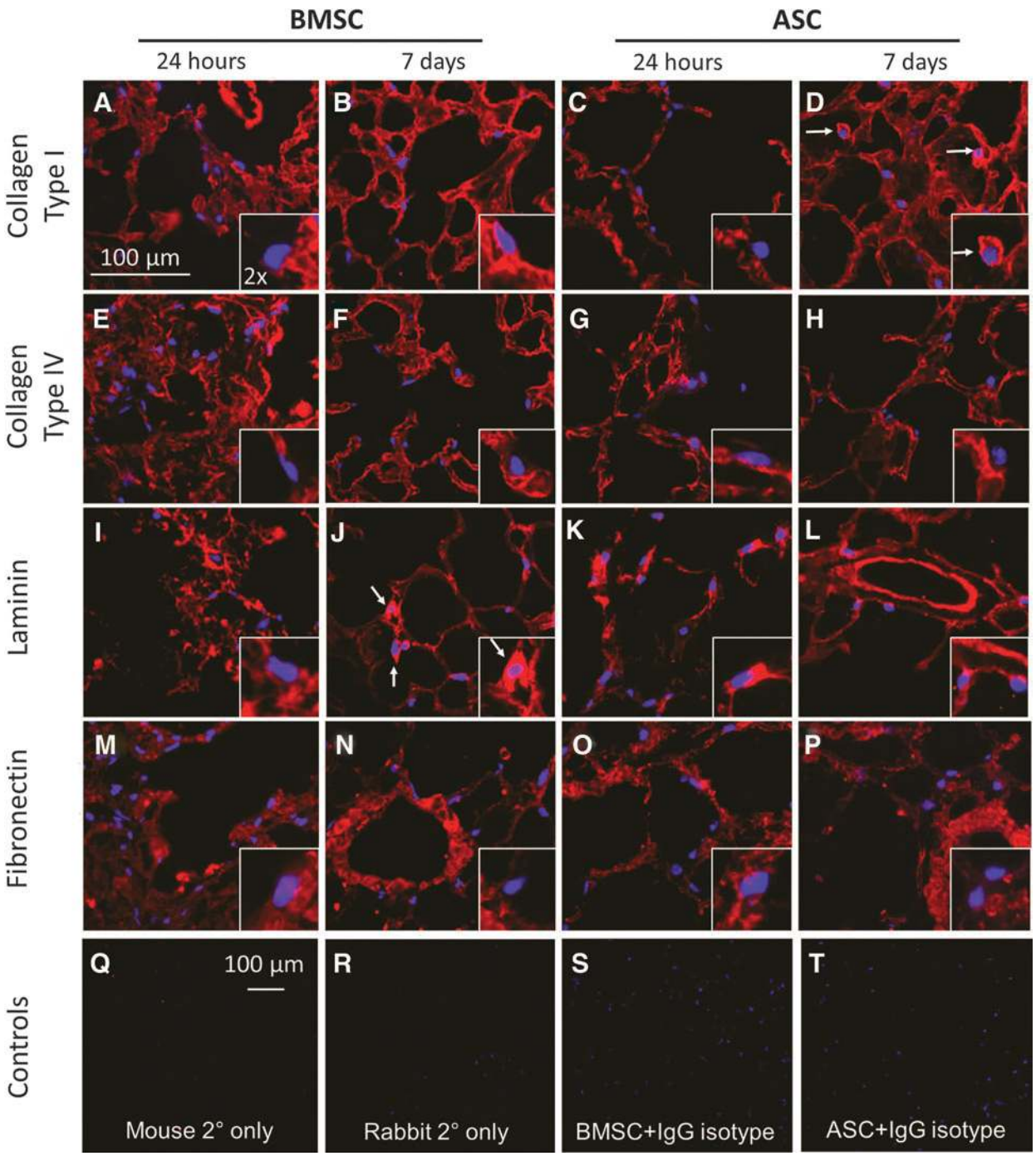

FIG. 7. ECM IHC in 3D slice cultures demonstrates the initial binding preferences of BMSC and ASC to the decellularized lung matrix. **(A–D)** A comparative analysis of these images suggests that association with collagen type I is marginal at 24 h for both cell types; however, at 7 days, the ASC show some association with areas identified as being dense in collagen type I and display a cell body-like silhouette of positive staining **(D**, white arrows). **(I–J)** BMSC seem to be associated with laminin dense areas by day 7 with cell body-like positive staining **(J,** white arrows**)** but do not initially show any particular preference for this protein. **(K, L)** At 24 h, ASC show close association with laminin-dense areas, and this association is reduced by day 7. No change in ECM-specific association or cell body-like staining is evident for the ubiquitous collagen IV **(E–H)** or the predominantly vascular-associated fibronectin **(M–P)** at 24 h or at 7 days after seeding of either cell type. **(Q–T)** Secondary antibody-only **(Q, R)** and IgG isotype **(S, T)** controls validate staining specificity. Note that **(A–P)** = 400× magnification and **(Q–T)** = 100× magnification. Insets represent a 2× enlarged portion of each field to show fine details. Color images available online at www.liebertpub.com/tea

Using a modification of this method, rhesus acellular lung scaffolds were routinely and consistently produced in our laboratory. The characterization of these NHP scaffolds demonstrated maintenance of lung ultrastructure and retention of ECM proteins, including collagen I, collagen IV, laminin, and fibronectin, as well as sulfated GAG. Most of the proteins appeared to retain their physiological organization after decellularization, as noted by IHC, with the exception of fibronectin, which appeared moth-eaten. This finding was further substantiated by Western blot analysis, which showed that sodium dodecyl sulfate (SDS)–reduced fibronectin produced smeared immunoreactive bands consistent with degradation. GAG content is retained in macaque lungs after decellularization in contrast to current rodent models that demonstrate substantial loss of GAG in lungs similarly decellularized by Triton/SDC, SDS, and CHAPS.[4,6,7] In fact, when normalized to the sample protein concentration, decellularized macaque lungs show a trend (not statistically significant) toward having higher GAG content. This normalization of the data is necessary in macaque lung specimens due to the requirement of using biopsies to quantify GAG rather than using whole lungs, which is much easier to accomplish in rodent models. The difference, although not significant, in the ratio of GAG to total protein between native and decellularized lungs may be explained by the fact that cellular proteins vastly contribute to the total protein content in native lungs; therefore, the ratio of GAG to total proteins in native would be expectedly less than that of the decellularized samples in which the total protein content is predominantly GAG-containing ECM. Given the size difference between rodent and primate lungs and the fact that the relative tissue thickness of primate lungs is much greater than that of rodents, it may be inferred that the macaque lung tissue, especially the underlying epithelial and connective tissue layers, incurs a milder insult by the detergents than do rodent lungs based simply on the differential ability of the detergents to diffuse through these two very different tissue specimens. A more in-depth analysis of the molecular mechanisms of decellularization would be beneficial in answering this question.

It is unknown whether protein disruption or degradation will have substantial effects on the eventual recellularization of these decellularized tissues or the differentiation of repopulating cells. No decellularization protocol is perfect; the use of detergents to decellularize any tissue will produce some deleterious effects on the proteins of the ECM.[17] The question to answer in moving forward with this technology is whether these effects will perturb the as yet unidentified "zip code" effect in which cells may potentially be guided in their differentiation by ECM–cell signaling interactions facilitated by the specific make-up of the organ-specific ECM to which the cells are seeded. Alternatively, ECM scaffolds may have greater benefit as complex 3D physical surfaces onto which cells primed for tissue-specific differentiation may be used to recapitulate the scaffold's tissue of origin. Recent publications describing bioartificially regenerated rodent lungs do not include in-depth analyses of the biochemical nature of the decellularized scaffolds, but rather they focus on the mechanical properties of the engineered tissue.[4,6,18] While these aspects are certainly warranted and hugely important, more thorough investigation is needed to determine the best methods for developing whole-organ tissue engineering toward the goal of human clinical applicability. Petersen *et al.* and Daly *et al.* provide excellent quantitative details of ECM proteins and sulfated GAG in decellularized lung scaffolds from rats and mice, respectively, but significant challenges arise when applying these sorts of assays to large organs.[7,19] For example, quantification of proteins and GAG in macaque lung relies on biopsy sampling since the size of the whole organ is so large. In addition, regional differences in the distribution of these biochemical components may contribute to widely varied results based on which region of the organ was sampled. Moreover, some lung tissues may be more resistant to decellularization-mediated degradation than others (e.g., thick air-conducting passages vs. thin alveolar tissue), and may therefore also yield varying results.

Dr. Stephen Badylak and colleagues have produced highly in-depth overviews of the various decellularization processes for multiple organs and have outlined the general criteria by which scientists should abide when creating decellularized biologic scaffolds. Crapo *et al.* state: "It should be understood that every cell removal agent and method will alter ECM composition and cause some degree of ultrastructure disruption. Minimization of these undesirable effects rather than complete avoidance is the objective of decellularization. […] The threshold of residual cellular material within ECM sufficient to elicit a negative remodeling response has not been investigated in detail and may vary depending upon ECM source, tissue type into which the ECM is implanted, and host immune function".[17] In our macaque model, we demonstrated a reduction in DNA content equivalent to an order of magnitude in decellularized macaque lung tissue relative to that of native lung. Of that small quantity of remaining DNA, gel electrophoresis analysis showed that this nuclear material was composed of highly fragmented, low-molecular-weight nuclear material consistent with recently described criteria.[17,20] It should be noted that in order to visualize the DNA recovered from decellularized macaque lungs, it was necessary to concentrate the remnant DNA by sodium acetate/ethanol precipitation in order to load an equal amount to the DNA recovered from native lungs; that is, without concentration, the minuscule amount of DNA from decellularized lungs would not be visible by gel electrophoresis.

Many cellular remnant proteins were detected by proteomics analysis of decellularized macaque lung specimens. It is unknown as to whether or not these components will adversely affect putative cell types chosen to re-seed the organ scaffolds or, ultimately, the host recipient of the regenerated organ. It is logical to postulate that these components will not remain in the matrix scaffold throughout the duration of regeneration; that is, cells seeded into the scaffold may likely absorb remnant cellular proteins, metabolize them, and recycle the amino acids for the production of new cellular or ECM materials—the same may be said of the remaining ECM proteins, for that matter. Future investigations are warranted to address these issues and to identify the mechanisms by which regenerative cells will adapt to and remodel their environment within the matrix scaffold.

While decellularized macaque lung alveolar parenchyma occupied similar histological area as that of native lungs, the MLI was slightly but significantly lower ($35.6\% \pm 12.0\%$ lower, $p < 0.0001$) in the decellularized lungs relative to native lungs. We speculate that decellularized lungs, while maintaining structural and organizational morphology

relative to native lungs, have undergone harsh treatment to remove cells, and even a small disruption of the elastic fibers within the ECM of the alveolar septae might result in some degree of relaxation of the air sacs and a slightly increased luminal diameter. Daly *et al.* showed that mouse lungs maintain overall percent parenchyma relative to airspace after decellularization despite substantial loss of elastin.[7] Ott *et al.* demonstrated, in decellularized rat lungs, that fractional volume of airspace and alveoli was increased.[4] These differences in macaques and rodents may be attributed to the condition of other ECM components after decellularization or the effect of size-related physical forces exerted on the relatively large macaque lungs during decellularization in contrast to small rodent lungs. Future experiments will be important to determine whether repopulation of the lung matrix with cells, which are capable of creating their surrounding matrix under the appropriate conditions, will result in reconstitution of proper elasticity in macaque as well as rodent tissue.

The use of stem cells in regenerative medicine has generated extensive interest because of their ability to differentiate into diverse cell lineages and their ease of isolation from embryos or adult tissues such as bone marrow and adipose tissue.[21] Both ESC and MSC from umbilical cord blood and adult bone marrow have been shown to differentiate into respiratory epithelial cells *in vitro*.[22–25] Functional bioartificial tissue regeneration will rely on the interaction of these cells with the ECM proteins of de-cellularized organ scaffolds. Recent studies have shown that the ECM contributes to the functional behavior of MSC and may be essential in guiding cell fate during tissue-specific differentiation.[26,27]

Macchiarini *et al.* have recently achieved clinical success using autologous bone marrow MSC and nasal epithelium for chondrocyte and luminal epithelium regeneration, respectively, to create bioartificial airways from decellularized cadaveric tracheas.[28–32] Although very encouraging, it is not yet known if a similar approach will be successful in regenerating the distal lung, as data regarding the differentiation of adult-derived MSC into the pulmonary lineage, as referenced above, is limited. Cortiella *et al.* cultured freeze/thaw- and detergent-decellularized rat lungs seeded with murine ESCs for 14–21 days and noted that the cells began to produce laminin and collagen type IV, which were substantially lost during the decellularization process.[9] Moreover, during this culture time, the cells showed region-specific expression of smooth muscle actin, cytokeratin 18, and CC10 in trachea and bronchi, supporting the notion that the natural lung matrix can influence the maturation of stem cells into lung-specific phenotypes. Daly *et al.* used murine BMSC to repopulate decellularized mouse lung matrices.[7] These cells persisted up to 28 days in 3D culture but showed only transient expression of the lung-specific thyroid transcription factor-1 (TTF-1). Together, these studies support the use of stem cells for investigating the repopulation of acellular lung matrices toward the goal of regenerating functional pulmonary tissue.

Here, macaque acellular lung scaffolds were successfully seeded with MSC isolated from the adult rhesus bone marrow (BMSC) and adipose tissue (ASC). Both cells were able to attach, elongate, and proliferate within the acellular lung scaffold *in vitro*. Similar observations were made between these two cell types, confirming that MSC from different sources have equivalent potential to repopulate acellular lung matrices. Various laminin isoforms are essential for pattern development and branching morphogenesis in lung development in murine models.[33–35] In a previous publication, our group found that murine BMSC initially adhered to areas rich in collagen type I and laminin but also in fibronectin-rich areas when seeded into acellular mouse lung scaffolds and begin producing these proteins themselves.[7] In macaque, we found by IHC that both BMSC and ASC showed a marked preference only for laminin above collagen types I and IV and fibronectin from 0 to 7 days in culture. This contrast between the current work and previous findings in rodent models highlights potential interspecies differences in the mechanisms of tissue regeneration. Future assays need to be developed to determine whether seemingly cell-associated ECM proteins are actually remnants from scaffold ECM, newly produced ECM, or partially degraded scaffold ECM being taken up and metabolized by the cells.

Collagen type I-specific cell binding data from the cell–ECM binding array suggests in higher degree of initial cell binding to this protein in contrast to what we observed in stem cell-seeded slice cultures *in situ*. Also, neither BMSC nor ASC showed substantial laminin-binding activity in the ECM array assay. It may be inferred, therefore, that the cell–ECM association preferences noted in the slice culture IHC staining may be a product of multiple ECM–cell signaling pathways stimulated by a combination of matrix proteins present in the decellularized scaffold in contrast to the single ECM proteins under analysis in the *in vitro* array. Moreover, the cell-binding array is performed in a microtiter plate on a surface of cell culture plastic. This surface has a substantially higher rigidity than natural lung matrix does; therefore, cells may have different attachment properties when compared to 3D matrix cultures.[36,37] To validate the data herein showing the relative positioning of rhesus BMSC and ASC within the acellular lung matrix, further studies will be necessary to elucidate the mechanisms by which MSC bind to and interact with the lung-derived scaffolds to reconstitute the native tissue. Ode and colleagues have provided an excellent profile of human MSC integrin expression and a morphological characterization of the functional behavior of MSC on various ECM proteins.[26] A similar integrin expression profile of rhesus MSC as well as integrin inhibition studies may provide clues as to the preferential interactions of MSC with the parenchymal and vascular ECM, which may help tailor tissue-engineering approaches using these cells.[26,38]

An important consideration toward the applicability of stem cells in lung regeneration is their ability to differentiate along pulmonary lineages. ESC can differentiate into a multitude of cell lineages, including respiratory epithelium.[22,39] Notably, Cortiella *et al.* demonstrated cells with a variety of immunophenotypes after seeding of acellular rat lung scaffolds with mouse ESCs.[9] Different cells expressed a number of lung-specific markers, including TTF-1, surfactant protein C (SpC), and Clara cell protein 10 (CCP10) as well as the endothelial and smooth muscle markers PECAM-1/CD31 and α-actin, respectively.[9] These results need to be further explored; however, for human clinical applicability, the use of allogenic ESC is less conceptually feasible than use of adult-derived MSC or induced pluripotent stem cells.[40] Bone marrow-derived MSC have the capacity to differentiate into airway epithelial cells (AEC) when cocultured with

mature AEC, *in vitro*, and others have shown that MSC can incorporate into lung epithelium *in vivo*.[25,41] Although MSC have thus far been limited to *in vitro* differentiation into bone, adipose, cartilage, and muscle/tendon,[42,43] much work is underway to expand their growth and differentiation capacities.[26,27] Alternatively, MSC may be more useful for providing a stroma and helping remodel the de-cellularized scaffold matrix as a platform for inoculation with other cell types. More investigation is needed to determine the most appropriate use of these cell types for the purposes of pulmonary regeneration.

The use of slice cultures is a useful tool for investigating the interaction of seeded cells with the decellularized lung parenchyma; however, for tissue recellularization to be successful, it is generally accepted that the *in vitro* conditions must mimic those of development. Therefore, the most appropriate models of distal lung bioengineering will be those that incorporate cellular, chemical, spatial, and mechanical cues to stimulate pulmonary differentiation. Lung-specific culture conditions in the context of whole-organ bioreactors may be effective for achieving the goal of lung regeneration. More basic as well as translational research is needed to develop these technologies in order to bring beneficial tissue products to the clinic.

Conclusion

This study demonstrates, for the first time, the applicability and clinical relevance of using the NHP rhesus macaque as a model in which to investigate whole-organ decellularization as a means to acquire biologic scaffolds for lung regeneration. Further studies will optimize the recellularization of macaque-derived lung scaffolds with stem cells, respiratory cells, and endothelial cells toward the goal of achieving successful implantation of functional pulmonary tissue produced in the laboratory.

Acknowledgments

The authors would like to thank the Division of Comparative Pathology as well as Cyndi Trygg and Jessica Eiermann of the Division of Regenerative Medicine at the Tulane National Primate Research Center for their assistance in acquiring and preparing rhesus macaque tissues. This work was supported in part by the National Center for Research Resources, NIH, Grant Number RR00164, the National Heart, Lung, and Blood Institute (NIH) T-32 Program Grant Number 5T32HL007973-07, NIH/RCMI Grant 5G12RR026260-03, NIH ARRA RC4HL106625 (DJW), NHLBI R21HL094611, the UVM Lung Biology COBRE (NIH NCRR P20 RR-155557, C Irvin PI), and Health Resources and Services Administration Contract 234-2005-37011C.

Disclaimer

The content is the responsibility of the authors alone and does not necessarily reflect the views or policies of the Department of Health and Human Services, nor does mention of trade names, commercial products, or organizations imply endorsement by the U.S. Government.

Disclosure Statement

No competing financial interests exist.

References

1. Organ Procurement and Transplantation Network (OPTN). Available at http://optn.transplant.hrsa.gov (accessed 13 April 2012.).
2. Ott, H.C., Matthiesen, T.S., Goh, S.K., Black, L.D., Kren, S.M., Netoff, T.I., and Taylor, D.A. Perfusion-decellularized matrix: using nature's platform to engineer a bioartificial heart. Nat Med **14,** 213, 2008.
3. Badylak, S.F., Taylor, D., and Uygun, K. Whole-organ tissue engineering: decellularization and recellularization of three-dimensional matrix scaffolds. Annu Rev Biomed Eng **13,** 27, 2010.
4. Ott, H.C., Clippinger, B., Conrad, C., Schuetz, C., Pomerantseva, I., Ikonomou, L., Kotton, D., and Vacanti, J.P. Regeneration and orthotopic transplantation of a bioartificial lung. Nat Med **16,** 927, 2010.
5. Price, A.P., England, K.A., Matson, A.M., Blazar, B.R., and Panoskaltsis-Mortari, A. Development of a decellularized lung bioreactor system for bioengineering the lung: the matrix reloaded. Tissue Eng Part A **16,** 2581, 2010.
6. Petersen, T.H., Calle, E.A., Zhao, L., Lee, E.J., Gui, L., Raredon, M.B., Gavrilov, K., Yi, T., Zhuang, Z.W., Breuer, C., Herzog, E., and Niklason, L.E. Tissue-engineered lungs for *in vivo* implantation. Science **329,** 538, 2010.
7. Daly, A.B., Wallis, J.M., Borg, Z.D., Bonvillain, R.W., Deng, B., Baliff, B.A., Jaworski, D.M., Allen, G.B., and Weiss, D. Initial binding and re-cellularization of de-cellularized mouse lung scaffolds with bone marrow-derived mesenchymal stromal cells. Tissue Eng Part A **18,** 1, 2012.
8. Song, J.J., Kim, S.S., Liu, Z., Madsen, J.C., Mathisen, D.J., Vacanti, J.P., and Ott, H.C. Enhanced *in vivo* function of bioartificial lungs in rats. Ann Thorac Surg **92,** 998, 2011.
9. Cortiella, J., Niles, J., Cantu, A., Brettler, A., Pham, A., Vargas, G., Winston, S., Wang, J., Walls, S., and Nichols, J.E. Influence of acellular natural lung matrix on murine embryonic stem cell differentiation and tissue formation. Tissue Eng Part A **16,** 2565, 2010.
10. Hollander, A.P., Atkins, R.M., Eastwood, D.M., Dieppe, P.A., and Elson, C.J. Human cartilage is degraded by rheumatoid arthritis synovial fluid but not by recombinant cytokines *in vitro*. Clin Exp Immunol **83,** 52, 1991.
11. Barbosa, I., Garcia, S., Barbier-Chassefiere, V., Caruelle, J.P., Martelly, I., and Papy-Garcia, D. Improved and simple micro assay for sulfated glycosaminoglycans quantification in biological extracts and its use in skin and muscle tissue studies. Glycobiology **13,** 647, 2003.
12. Izadpanah, R., Joswig, T., Tsien, F., Dufour, J., Kirijan, J.C., and Bunnell, B.A. Characterization of multipotent mesenchymal stem cells from the bone marrow of rhesus macaques. Stem Cells Dev **14,** 440, 2005.
13. Izadpanah, R., Trygg, C., Patel, B., Kriedt, C., Dufour, J., Gimble, J.M., and Bunnell, B.A. Biologic properties of mesenchymal stem cells derived from bone marrow and adipose tissue. J Cell Biochem **99,** 1285, 2006.
14. Zuk, P.A., Zhu, M., Ashjian, P., De Ugarte, D.A., Huang, J.I., Mizuno, H., Alfonso, Z.C., Fraser, J.K., Benhaim, P., and Hedrick, M.H. Human adipose tissue is a source of multipotent stem cells. Mol Biol Cell **13,** 4279, 2002.
15. Gibbs, R.A., Rogers, J., Katze, M.G., Bumgarner, R., Weinstock, G.M., Mardis, E.R., Remington, K.A., Strausberg, R.L., Venter, J.C., Wilson, R.K., Batzer, M.A., Bustamante, C.D., Eichler, E.E., Hahn, M.W., Hardison, R.C., Makova, K.D., Miller, W., Milosavljevic, A., Palermo, R.E., Siepel, A., Sikela, J.M., Attaway, T., Bell, S., Bernard, K.E., Buhay, C.J., Chan-

drabose, M.N., Dao, M., Davis, C., Delehaunty, K.D., Ding, Y., Dinh, H.H., Dugan-Rocha, S., Fulton, L.A., Gabisi, R.A., Garner, T.T., Godfrey, J., Hawes, A.C., Hernandez, J., Hines, S., Holder, M., Hume, J., Jhangiani, S.N., Joshi, V., Khan, Z.M., Kirkness, E.F., Cree, A., Fowler, R.G., Lee, S., Lewis, L.R., Li, Z., Liu, Y.S., Moore, S.M., Muzny, D., Nazareth, L.V., Ngo, D.N., Okwuonu, G.O., Pai, G., Parker, D., Paul, H.A., Pfannkoch, C., Pohl, C.S., Rogers, Y.H., Ruiz, S.J., Sabo, A., Santibanez, J., Schneider, B.W., Smith, S.M., Sodergren, E., Svatek, A.F., Utterback, T.R., Vattathil, S., Warren, W., White, C.S., Chinwalla, A.T., Feng, Y., Halpern, A.L., Hillier, L.W., Huang, X., Minx, P., Nelson, J.O., Pepin, K.H., Qin, X., Sutton, G.G., Venter, E., Walenz, B.P., Wallis, J.W., Worley, K.C., Yang, S.P., Jones, S.M., Marra, M.A., Rocchi, M., Schein, J.E., Baertsch, R., Clarke, L., Csuros, M., Glasscock, J., Harris, R.A., Havlak, P., Jackson, A.R., Jiang, H., Liu, Y., Messina, D.N., Shen, Y., Song, H.X., Wylie, T., Zhang, L., Birney, E., Han, K., Konkel, M.K., Lee, J., Smit, A.F., Ullmer, B., Wang, H., Xing, J., Burhans, R., Cheng, Z., Karro, J.E., Ma, J., Raney, B., She, X., Cox, M.J., Demuth, J.P., Dumas, L.J., Han, S.G., Hopkins, J., Karimpour-Fard, A., Kim, Y.H., Pollack, J.R., Vinar, T., Addo-Quaye, C., Degenhardt, J., Denby, A., Hubisz, M.J., Indap, A., Kosiol, C., Lahn, B.T., Lawson, H.A., Marklein, A., Nielsen, R., Vallender, E.J., Clark, A.G., Ferguson, B., Hernandez, R.D., Hirani, K., Kehrer-Sawatzki, H., Kolb, J., Patil, S., Pu, L.L., Ren, Y., Smith, D.G., Wheeler, D.A., Schenck, I., Ball, E.V., Chen, R., Cooper, D.N., Giardine, B., Hsu, F., Kent, W.J., Lesk, A., Nelson, D.L., O'Brien W, E., Prufer, K., Stenson, P.D., Wallace, J.C., Ke, H., Liu, X.M., Wang, P., Xiang, A.P., Yang, F., Barber, G.P., Haussler, D., Karolchik, D., Kern, A.D., Kuhn, R.M., Smith, K.E., and Zwieg, A.S. Evolutionary and biomedical insights from the rhesus macaque genome. Science **316,** 222, 2007.

16. Sekhon, H.S., Keller, J.A., Benowitz, N.L., and Spindel, E.R. Prenatal nicotine exposure alters pulmonary function in newborn rhesus monkeys. Am J Respir Crit Care Med **164,** 989, 2001.
17. Crapo, P.M., Gilbert, T.W., and Badylak, S.F. An overview of tissue and whole organ decellularization processes. Biomaterials **32,** 3233, 2011.
18. Song, J.J., and Ott, H.C. Organ engineering based on decellularized matrix scaffolds. Trends Mol Med **17,** 424, 2011.
19. Petersen, T.H., Calle, E.A., Colehour, M.B., and Niklason, L.E. Matrix composition and mechanics of decellularized lung scaffolds. Cells Tissues Organs **195,** 222, 2012.
20. Keane, T.J., Londono, R., Turner, N.J., and Badylak, S.F. Consequences of ineffective decellularization of biologic scaffolds on the host response. Biomaterials **33,** 1771, 2012.
21. Kørbling, M., and Estrov, Z. Adult stem cells for tissue repair—a new therapeutic concept? N Engl J Med **349,** 570, 2003.
22. Rippon, H.J., Polak, J.M., Qin, M., and Bishop, A.E. Derivation of distal lung epithelial progenitors from murine embryonic stem cells using a novel three-step differentiation protocol. Stem Cells **24,** 1389, 2006.
23. Berger, M.J., Adams, S.D., Tigges, B.M., Sprague, S.L., Wang, X.J., Collins, D.P., and McKenna, D.H. Differentiation of umbilical cord blood-derived multilineage progenitor cells into respiratory epithelial cells. Cytotherapy **8,** 480, 2006.
24. Samadikuchaksaraei, A., Cohen, S., Isaac, K., Rippon, H.J., Polak, J.M., Bielby, R.C., and Bishop, A.E. Derivation of distal airway epithelium from human embryonic stem cells. Tissue Eng **12,** 867, 2006.
25. Wang, G., Bunnell, B.A., Painter, R.G., Quiniones, B.C., Tom, S., Lanson, N.A., Jr., Spees, J.L., Bertucci, D., Peister, A., Weiss, D.J., Valentine, V.G., Prockop, D.J., and Kolls, J.K. Adult stem cells from bone marrow stroma differentiate into airway epithelial cells: potential therapy for cystic fibrosis. Proc Natl Acad Sci U S A **102,** 186, 2005.
26. Ode, A., Duda, G.N., Glaeser, J.D., Matziolis, G., Frauenschuh, S., Perka, C., Wilson, C.J., and Kasper, G. Toward biomimetic materials in bone regeneration: functional behavior of mesenchymal stem cells on a broad spectrum of extracellular matrix components. J Biomed Mater Res A **95A,** 1114, 2010.
27. Lindner, U., Kramer, J., Behrends, J., Driller, B., Wendler, N.O., Boehrnsen, F., Rohwedel, J., and Schlenke, P. Improved proliferation and differentiation capacity of human mesenchymal stromal cells cultured with basement-membrane extracellular matrix proteins. Cytotherapy **12,** 992, 2010.
28. Macchiarini, P., Jungebluth, P., Go, T., Asnaghi, M.A., Rees, L.E., Cogan, T.A., Dodson, A., Martorell, J., Bellini, S., Parnigotto, P.P., Dickinson, S.C., Hollander, A.P., Mantero, S., Conconi, M.T., and Birchall, M.A. Clinical transplantation of a tissue-engineered airway. Lancet **372,** 2023, 2008.
29. Asnaghi, M.A., Jungebluth, P., Raimondi, M.T., Dickinson, S.C., Rees, L.E., Go, T., Cogan, T.A., Dodson, A., Parnigotto, P.P., Hollander, A.P., Birchall, M.A., Conconi, M.T., Macchiarini, P., and Mantero, S. A double-chamber rotating bioreactor for the development of tissue-engineered hollow organs: from concept to clinical trial. Biomaterials **30,** 5260, 2009.
30. Jungebluth, P., Go, T., Asnaghi, A., Bellini, S., Martorell, J., Calore, C., Urbani, L., Ostertag, H., Mantero, S., Conconi, M.T., and Macchiarini, P. Structural and morphologic evaluation of a novel detergent-enzymatic tissue-engineered tracheal tubular matrix. J Thorac Cardiovasc Surg **138,** 586, 2009.
31. Go, T., Jungebluth, P., Baiguero, S., Asnaghi, A., Martorell, J., Ostertag, H., Mantero, S., Birchall, M., Bader, A., and Macchiarini, P. Both epithelial cells and mesenchymal stem cell-derived chondrocytes contribute to the survival of tissue-engineered airway transplants in pigs. J Thorac Cardiovasc Surg **139,** 437, 2010.
32. Baiguera, S., Jungebluth, P., Burns, A., Mavilia, C., Haag, J., De Coppi, P., and Macchiarini, P. Tissue engineered human tracheas for *in vivo* implantation. Biomaterials **31,** 8931, 2010.
33. Schuger, L., Varani, J., Killen, P.D., Skubitz, A.P., and Gilbride, K. Laminin expression in the mouse lung increases with development and stimulates spontaneous organotypic rearrangement of mixed lung cells. Dev Dyn **195,** 1992.
34. Schuger, L., O'Shea, S., Rheinheimer, J., and Varani, J. Laminin in lung development: effects of anti-laminin antibody in murine lung morphogenesis. Dev Biol **137,** 1990.
35. Nguyen, N.M., and Senior, R.M. Laminin isoforms and lung development: all isoforms are not equal. Dev Biol **294,** 271, 2006.
36. Throm Quinlan, A.M., Sierad, L.N., Capulli, A.K., Firstenberg, L.E., and Billiar, K.L. Combining dynamic stretch and tunable stiffness to probe cell mechanobiology *in vitro*. PLoS One **6,** e23272, 2011.
37. Han, J., Lazarovici, P., Pomerantz, C., Chen, X., Wei, Y., and Lelkes, P.I. Co-electrospun blends of PLGA, gelatin, and elastin as potential nonthrombogenic scaffolds for vascular tissue engineering. Biomacromolecules **12,** 399, 2011.
38. Semon, J.A., Nagy, L.H., Llamas, C.B., Tucker, H.A., Lee, R.H., and Prockop, D.J. Integrin expression and integrin-

mediated adhesion *in vitro* of human multipotent stromal cells (MSCs) to endothelial cells from various blood vessels. Cell Tissue Res **341,** 147, 2010.
39. Nishimura, Y., Hamazaki, T.S., Komazaki, S., Kamimura, S., Okochi, H., and Asashima, M. Ciliated cells differentiated from mouse embryonic stem cells. Stem Cells **24,** 1381, 2006.
40. Takahashi, K., and Yamanaka, S. Induction of pluripotent stem cells from mouse embryonic and adult fibroblast cultures by defined factors. Cell **126,** 663, 2006.
41. Loi, R., Beckett, T., Goncz, K.K., Suratt, B.T., and Weiss, D.J. Limited restoration of cystic fibrosis lung epithelium *in vivo* with adult bone marrow-derived cells. Am J Respir Crit Care Med **173,** 171, 2006.
42. Pittenger, M.F., Mackay, A.M., Beck, S.C., Jaiswal, R.K., Douglas, R., Mosca, J.D., Moorman, M.A., Simonetti, D.W., Craig, S., and Marshak, D.R. Multilineage potential of adult human mesenchymal stem cells. Science **284,** 143, 1999.
43. Short, B., Brouard, N., Occhiodoro-Scott, T., Ramakrishnan, A., and Simmons, P.J. Mesenchymal stem cells. Arch Med Res **34,** 565, 2003.

Address correspondence to:
Bruce A. Bunnell, Ph.D.
Department of Pharmacology
Center for Stem Cell Research and Regenerative Medicine
Tulane University School of Medicine
1430 Tulane Avenue, SL-99
New Orleans, LA 70112

E-mail: bbunnell@tulane.edu

Received: October 20, 2011
Accepted: June 18, 2012
Online Publication Date: August 22, 2012